Coherent Ising machine with quantum feedback: The total and conditional master equation methods

Simon Kiesewetter and Peter D. Drummond
Centre for Quantum Science and Technology Theory, Swinburne University of Technology, Melbourne 3122, Australia

(Received 2 March 2022; accepted 14 June 2022; published 12 August 2022)

We give a detailed theoretical derivation of the master equation for the coherent Ising machine. This is a quantum computational network with feedback, that approximately solves NP-hard combinatoric problems, including the traveling salesman problem and various extensions and analogs. There are two possible types of master equation, either conditional on the feedback current or unconditional. We show that both types can be accurately simulated in a scalable way using stochastic equations in the positive-P phase-space representation. This depends on the nonlinearity present, and we use parameter values that are typical of current experiments. While the two approaches are in excellent agreement, they are not equivalent with regard to efficiency. We find that unconditional simulation has much greater efficiency, and is more scalable to large sizes. This is a case where too much knowledge is a dangerous thing. Conditioning the simulations on the feedback current is not essential to determining the success probability, but it greatly increases the computational complexity. To illustrate the speed improvements obtained with the unconditional approach, we carry out full quantum simulations of the master equation with up to 1000 nodes.

DOI: 10.1103/PhysRevA.106.022409

I. INTRODUCTION

The coherent Ising machine (CIM) is a type of computational device which operates in a fundamentally different way from both classical and gate-based quantum computers. It has been known for a while that there is a wide variety of computationally challenging (NP-complete or NP-hard) [1,2] problems that can be mapped onto the Ising model. This is a simple model consisting of binary variables, usually identified with spins in a magnetic material which interact both locally and nonlocally to give a Hamiltonian model whose ground state is the solution to the computational problem. Originally, the model corresponded to spins interacting with an external magnetic field and with each other through spin-spin coupling. Since a true Ising model using physical spins is difficult to manipulate experimentally, the CIM aims to simulate it, using continuous variables in a nonequilibrium setup whose steady state closely resembles the Ising model. The largest experiments of this type [3] use a measurement-feedback strategy [4].

We compare two different techniques of simulating the measurement-feedback CIM using the positive-P phase-space representation [5,6], which is an exact mapping of quantum dynamics to stochastic equations. Phase-space simulation using the positive-P representation provides a convenient, scalable way to simulate the nonlinear system dynamics of some types of complex, dissipative quantum systems without the need to make approximations. Except for rare cases with very low losses, where nonvanishing boundary terms are present, this method gives quantitative predictions. We show that there is no need to make any approximations of the system equations [7–9]. However, simulating the system dynamics is complicated by the homodyne measurement used for feedback, which causes a partial collapse of the system wave function according to the measurement outcome.

The measurement outcome is partly determined by quantum noise at the measurement site. As a result, the quantum dynamics follows a conditional master equation due to the noisy outcome of the measurement feedback. Here we derive the multimode conditional master equation as a stochastic equation in the Stratonovich calculus. The operator associated with the wave-function collapse leads to terms which do not correspond to a conventional Fokker-Planck equation in a phase-space representation, and a weighted simulation is required [10]. It is also possible to consider an average over the feedback, giving an unconditional master equation. Both types of equation can be exactly simulated with the positive-P phase-space method, and we show that they lead to identical success rate predictions.

The original gedanken experiment [11–13] used laser pulses impinging on multiple degenerate parametric oscillators (DPOs) [6,14], realized by a nonlinear medium in an optical cavity. At a certain pump strength, each DPO becomes a bistable system, with quantum states that are associated with the binary variables of the Ising model, and can be coupled to each other. Hence, an ideal DPO-based CIM is a true quantum system, with transient states that are like a Schrödinger cat state of the form $|\alpha\rangle + |-\alpha\rangle$ [15–17], when losses are very low. Therefore, it has the potential to be subject to quantum enhancement, which may contribute to steering the system into the desired steady state, approximately equivalent to an Ising ground state. The significance of such effects is still subject to investigation. There are also other types of realization of the CIM via electronic or digital circuits that simulate the dynamics in a classical regime [18].

In the first practical realizations of the CIM the DPO itself was a localized pulse stored in an optical fiber loop [19,20]. Effective spin-spin interactions are obtained using an optical delay-line (ODL)-CIM that redirects part of the time-delayed signal back into the fiber loop, allowing different pulses to interact. While this architecture has many advantages, its principal disadvantage is that it is difficult to scale up to include large numbers of spins. Due to the close similarity of superconducting and optical parametric amplifiers, it may be feasible to realize this type of device in a superconducting waveguide. Much stronger quantum effects are known in such cases [21], and quantum tunneling is possible [22–24].

A different version of the CIM, commonly called a measurement-feedback or MFB CIM, was developed a few years later [3,4,25–27]. Here, the signal state is observed via a homodyne detector and the feedback strength is calculated electronically based on the measurement. A feedback signal is then generated from the pump pulse and fed back into the loop after a variable time delay. This architecture has the great advantage of being very well suited for the simulation of systems of a large number of Ising spins. It has been demonstrated most impressively in a recent experiment of a measurement-feedback-type CIM involving 100 000 spins [3].

Phase-space approaches have proved the only practical, scalable way to treat large quantum networks. These are based on earlier multimode quantum field simulations [28–30], and have already been used to analyze Gaussian boson sampling quantum computers [31]. Equations based on an approximate phase-space approach are known for an ODL-CIM [13,32] and for an MFB-CIM architecture [4]. These use a modified Wigner representation [33], which truncates third- and higher-order derivatives in the corresponding Fokker-Planck equation. Exact positive-P equations of motion [5] that do not require truncation are given both for the ODL [32,34] and for the MFB-type CIM [35]. A scheme for weighted phase-space simulations involving the conditional master equation of a MFB-type CIM is known [25]. Discrete-time descriptions of the MFB-type CIM have been published [26,36], which use a simplified Gaussian phase-space representation [37].

The term scalable refers here to the polynomial-time solution of the CIM simulations for the given parameters and feedback method. There is no evidence of sampling error limitations, but the observed efficient sampling may not hold for stronger couplings, or different feedback regimes. We do not claim that our method can accurately solve NP-hard problems in a polynomial time, which is generally regarded as impossible on a digital computer. However, these simulations provide a useful way to quantitatively understand the physics and expected performance of this quantum technology. Approximate but fast quantum hardware solutions of these types of problem can be extremely useful in practical applications. There can still be an experimental "quantum advantage" if classical polynomial-time simulation is slower than experiment.

In this article, after reviewing the topic of quantum measurement-feedback systems in general, we present two ways in which the system quantum dynamics can be simulated using exact phase-space techniques. These correspond to the conditional and unconditional master equations approaches. Full conditional simulation leads to an ensemble of weighted trajectories through which the quantum master equation conditioned on the feedback currents can be simulated [10]. It is a relatively complex method due to the fact that it requires a careful rebalancing of the weight distribution to prevent numerical instabilities from exponential growth in the weights. Alternatively, the full unconditional master equation can be treated using unweighted stochastic trajectories, which yields ensemble averages of quadrature measurements.

We compare the simulation outcomes and performance of the two methods. They agree with each other extremely well in modeling success rates of the feedback CIM. From a computational point of view, we find that the unconditional method is greatly preferred. As it requires computing and rebalancing weights, the conditional algorithm is more complex. This approach also requires orders of magnitude more stochastic trajectories to give accurate predictions. The large speed improvement in unconditional simulations is especially important in light of the large size of recent measurement-feedback-type CIM experiments.

II. THE COHERENT ISING MACHINE

A. The Ising model

The Ising model was formulated almost a century ago [38,39] to model ferromagnetism and related phenomena. It is a very simple theory, consisting of discrete variables σ_i, indicating the nuclei's magnetic spins. These are oriented either "up" or "down," corresponding to $\sigma = \pm 1$. The spins now interact with each other through spin-spin interaction and with an external magnetic field. The Ising model Hamiltonian is

$$H = -\sum_{i,j} J_{ij}\sigma_i\sigma_j - \sum_i h_i\sigma_i, \tag{2.1}$$

where $\mathbf{J}$ is the coupling matrix and h is proportional to the possibly inhomogeneous magnetic field strength.

Apart from its usefulness in explaining ferromagnetism, the Ising model has another interesting feature: a wide variety of computationally challenging (NP-complete or NP-hard) problems can be mapped onto it via changing the coupling matrix and investigating the corresponding ground state. As an example, consider the so-called max-cut problem (see Fig. 1). The problem statement is as follows:

Given an undirected graph $G = (V, E)$ where $V = \{v_i\}$ is the set of vertices and $E = \{e_i\}$ is the set of edges and a weight function $w : E \to \mathbb{R}^+$, find the bipartition (cut) into sets $V = U \uplus W$ with the highest sum of "weights along the cut line," that is, maximize $f \equiv \sum_i w(e_i)$, where $e_i = \{u, w\}, u \in U, w \in W$.

The way to map this problem onto the Ising model is to identify each vertex with a certain spin. The interaction matrix is set to the negative of the weights between the nodes (zero if there is no edge) and the external magnetic field is set to zero. The spin states then indicate whether a vertex belongs to set U or W. Upon inspecting the system Hamiltonian, one finds that

$$\begin{aligned} H &= -\sum_{i,j} J_{ij} + 2\sum_{(i,j)\in\Delta} J_{ij} \\ &= C + 2\sum_{(i,j)\in\Delta} J_{ij}, \end{aligned} \tag{2.2}$$

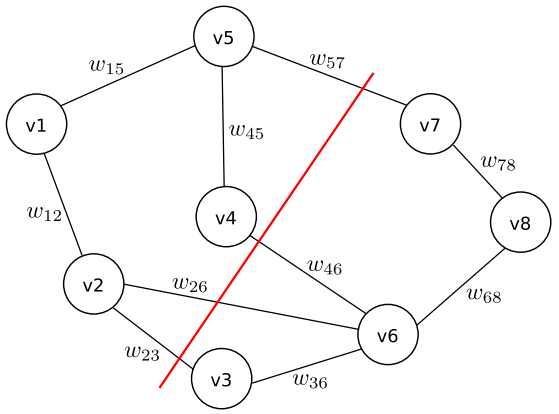

FIG. 1. Example of a max-cut problem. The red line indicates a proposed decomposition ("cut") into two graphs. The problem consists of bisecting the given graph while maximizing the sum of weights along the cut.

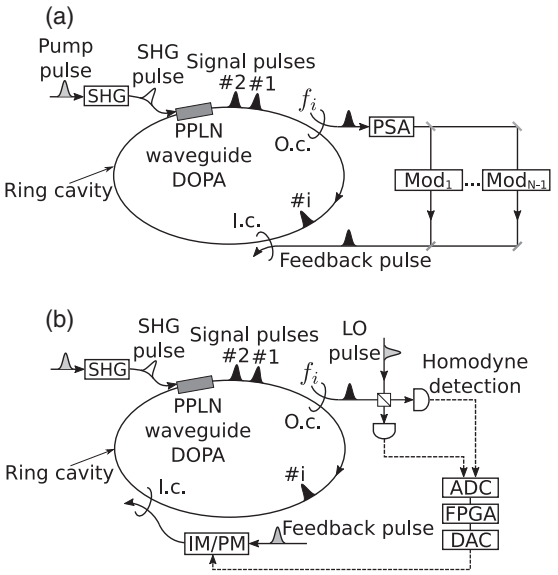

FIG. 2. Two different CIM architectures. (a) The optical delay lines type of the CIM. Here, the feedback is generated by redirecting part of the signal pulses through optical lines adjusted in length to match up with different pulses at the injection coupler site. (b) The measurement-feedback architecture, where the pulses are measured by a homodyne detector. The measurement is digitized and the feedback is calculated via an FPGA. Based on the calculation, an output pulse is generated which is redirected into the ring cavity. Here, "O.c." and "I.c." stand for "Output coupler" and "Injection coupler," respectively. Redrawn, following the original published figure in [40].

where Δ is the set of indices (i, j) such that $v_i \in U, v_j \in W$ or vice versa. Since the total sum of weights $C = -\sum_{i,j} J_{ij}$ is fixed, minimizing H will maximize the sum of "cut" weights (since $J_{ij} \leqslant 0$ by construction).

Due to the absence of Zeeman terms, the mapping between the max-cut problem and the Ising model is possibly the most natural and well-known one; however, a plethora of other interesting and computationally challenging ones can be mapped to the Ising model in a similar well.

It is perhaps surprising, given how ubiquitous systems that are described by the Ising model are in nature, that it could theoretically be used to facilitate solving all these computational problems. In light of this, is it possible to build a (special-purpose) computational machine, in which the calculation is "carried out" by magnetic spins and their interactions with each other and with an external magnetic field?

For such a machine, one would have to be able to (i) accurately set the interaction matrix $\mathbf{J}$ and external magnetic field h_i to arbitrary values; (ii) significantly reduce or mitigate the influence of external perturbations, such as thermal fluctuations; and (iii) accurately determine the spin states at the end of the "computation phase." These requirements alone already pose significant challenges if one attempted to use the magnetic spins of single atoms for which the Ising model was original formulated. Additionally, it might be desirable to control the initial state of the system as well as have some sort of mechanism to increase the chance of the system evolving into its ground state instead of a local minimum, which would constitute additional challenges.

B. CIM architectures

In the setup of the coherent Ising machine, a nonlinear material is embedded in a ring cavity. Instead of using multiple DPOs to represent the different spin states, the DPO is operated (pumped) in a pulsed way such that all spin states of the system are represented by the same DPO at different times. This means, for an Ising model with N spins, the DPO will represent the spin states σ_1 during the first pulse, σ_2 during the second pulse, etc., eventually representing σ_N, before representing σ_1 again in the next pulse.

The obvious missing ingredient is the interaction between spins, as specified by the $\mathbf{J}$ matrix as well as with the external magnetic field h_i. There are, as of the writing of this article, two ways by which this is achieved (see Fig. 2).

The first one is through optical delay lines [19]. Here, a part of the signal is extracted with an output coupler, amplified by a phase-sensitive amplifier and led through a number of optical lines before being fed back into the ring cavity with an injection coupler. These optical lines are adjusted in length such that two different optical pulses are produced when the delayed signal is fed back into the cavity. Within the delay lines, the signal is adjusted through amplification and phase shift to match the corresponding element of the $\mathbf{J}$ matrix.

In the second scheme [4], a part of the signal is continuously measured via a homodyne detector. The appropriate feedback signal is then calculated electronically. Based on this, the feedback signal is generated separately through an intensity modulator and a phase modulator acting on the laser beam which feeds the pump pulse. The injected signal is fed back into the ring cavity. The calculation of the feedback signal is carried out via a field-programmable gate array (FPGA) to minimize computation times. It might seem counterintuitive to use electronic circuitry, here an FPGA, for the calculation of the feedback signal—after all, is not the goal of the coherent Ising machine to design a computational device based on physical processes other than (semiconductor) electronics?

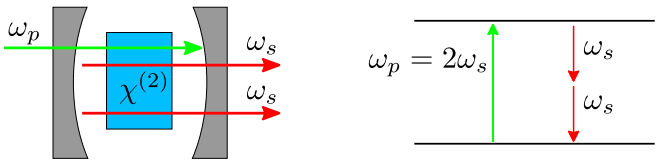

FIG. 3. Schematic figure of a degenerate parametric oscillator on resonance. Through parametric down-conversion taking place inside the optical cavity, absorption of a single pump photon results in two signal photons with half its frequency.

However, the FPGA only computes a part of the problem, namely, the magnitude of the interaction strength, while the rest of the computation still happens "inside" the ring cavity. On the other hand, the measurement-feedback-based CIM architecture has significant advantages over the optical delay lines architecture as well.

The main advantage of the optical delay lines architecture is very fast operating times since no complicated logical gates, such as an FPGA, are involved in the calculation of the feedback strength. However, for an Ising model with N spins and a dense $\mathbf{J}$ matrix, up to $N-1$ optical delay lines are required. Hence, there are inherent limitations on scalability. Conversely, for the measurement-feedback architecture, the FPGA poses a bottleneck in operating time. At the same time, the system can be scaled up to include a large number of spin states very easily due to the absence of optical delay lines, which was demonstrated recently by an experiment of a CIM involving 100 000 spin states [3]. Additionally, the measurement-feedback scheme provides greater flexibility, which makes it possible to simulate more exotic systems, such as Ising-like models that include interactions between three or more spins, and sophisticated protocols to increase the likelihood of reaching the ground state.

In this paper, we obtain a complete quantum description and a way of simulating the measurement-feedback type of the CIM.

In the measurement-feedback architecture, the signal states are continuously measured. Based on the measurement result, an FPGA calculates the appropriate feedback based on the Ising model terms. Based on this calculation, a separate signal is created and injected into the cavity. Due to the continuous homodyne measurement that the signal states are subject to, the wave function experiences a continuous partial state collapse conditional on the measurement outcome. This makes the formulation of the system equations for the MFB-type CIM a more complex task compared to the ODL architecture, as it involves the theory of measurement-feedback quantum systems. In the following sections we first describe a simple model of the individual DPO components, and a general approach describing how to couple these via quantum measurement-feedback theory.

III. DEGENERATE PARAMETRIC OSCILLATOR

In place of physical spins, the coherent Ising machine uses a degenerate parametric oscillator (see Fig. 3) [6,41]. In present experiments each DPO is a multimode, pulsed system due to its traveling-wave nature [29,42]. However, to simplify the theory, it is common to use a single-mode intracavity model. This treats each DPO as a single supermode, which is often valid classically [43,44], although a full multimode treatment is required to treat all quantum noise effects, even in mode-locked systems [45,46]. While simpler than current fiber-optic experiments, the single-mode model treats the most important features. It could in principle be implemented more precisely in future experiments.

A. Single-mode DPO theory

As discussed above, we regard the CIM as a network of single-mode DPOs. Each is essentially a $\chi^{(2)}$ nonlinear medium embedded in an optical or microwave cavity. It is driven (pumped) by a laser at frequency ω_p. Due to the nonlinear medium, parametric down-conversion can occur, which leads to the creation of two photons with frequencies ω_s and ω_i. Subsequently, we assume that $\omega_i = \omega_s = \omega_p/2$ and that the cavity is resonant to both ω_p and ω_s. How can a nonlinear medium inside an optical cavity then take the place of a discrete magnetic spin?

In order to understand this, we first consider a DPO driven by a pump field with induced amplitude $\mathcal{E}_p$, which is subject to a decay rate γ_p, while photons created through parametric down-conversion, which we subsequently call the signal field, are subject to a decay rate γ_s. The DPO Hamiltonian is

$$H_{DPO} = i\hbar\frac{\kappa}{2}\left[a_p(a_s^\dagger)^2 - a_p^\dagger a_s^2\right] + i\hbar\left[\mathcal{E}_p a_p^\dagger - \mathcal{E}_p^* a_p\right], \quad (3.1)$$

where a_p and a_s are the pump and signal field operators, respectively, and κ is a nonlinearity parameter of the medium. Before using a more complete quantum description later, we first consider the evolution of the system in a classical picture. For this, we first write down the Heisenberg-Langevin equations for the expectation values of a_p and a_s, with the definitions that $\alpha = \langle a_s\rangle$ and $\alpha_p = \langle a_p\rangle$.

To give an initial intuition about the behavior, we start by assuming that expectation values factorize coherently, $\langle a_s^\dagger a_p\rangle = \alpha_s^*\alpha_p$ and $\langle a_s^2\rangle = \alpha_s^2$, which gives

$$\begin{aligned}\frac{d}{dt}\alpha_s &= -\gamma_s\alpha_s + \kappa\alpha_s^*\alpha_p,\\ \frac{d}{dt}\alpha_p &= \mathcal{E}_p - \gamma_p\alpha_p - \frac{1}{2}\kappa\alpha_s^2\,.\end{aligned} \quad (3.2)$$

One finds three steady-state solutions for Eqs. (3.2):

$$\begin{aligned}\alpha_s &= 0,\\ \alpha_p &= \mathcal{E}_p/\gamma_p,\end{aligned} \quad (3.3)$$

as well as

$$\begin{aligned}\alpha_s &= \pm\sqrt{\frac{2}{\chi}\left[\mathcal{E}_p - \frac{\gamma_p\gamma_s}{\kappa}\right]},\\ \alpha_p &= \frac{\gamma_s}{\kappa}\,.\end{aligned} \quad (3.4)$$

A second-derivative test reveals that Eqs. (3.3) contain the only stable steady-state solution for $\mathcal{E}_p < \mathcal{E}_{p,th}$, with $\mathcal{E}_{p,th}$ called the threshold pump strength defined as $\mathcal{E}_{p,th} = \frac{\gamma_s\gamma_p}{\kappa}$, whereas for $\mathcal{E}_p > \mathcal{E}_{p,th}$, Eqs. (3.3) are an unstable solution and Eqs. (3.4) are both stable solutions. In the coherent Ising

machine, the two distinct solutions of the DPO operated in the above-threshold regime take the place of the discrete spin states.

B. Quantum dynamics in phase space

The CIM is operated in a pulsed way with time-multiplexed spin states. It nevertheless lends itself to a description of multiple DPO states interacting simultaneously. This has an enormous Hilbert space. Conventional number state expansions cannot be used in these cases, due to the exponentially large basis set. It is therefore essential to use a probabilistic approach in phase space. This has been used in a number of very large-scale quantum simulations [31,47].

Here, we want to analyze the phase-space dynamics of the system in detail. Before looking at the multispin case, we will summarize known results for the single-DPO system [6]. We consider the scenario where the DPO is driven by an induced pump rate of $\mathcal{E}_p$ and the pump and signal field are subject to a decay rate of γ_p and γ_s, respectively. The system evolution is described by the quantum master equation

$$\frac{d}{dt}\rho = \gamma_p \mathcal{D}[a_p]\rho + \gamma_s \mathcal{D}[a_s]\rho + \frac{1}{i\hbar}[H_{DOPO}, \rho]. \quad (3.5)$$

The nonunitary evolution or mode damping is described by the superoperator $\mathcal{D}[c]\rho \equiv 2c\rho c^\dagger - (c^\dagger c\rho + \rho c^\dagger c)$, which treats loss through the mirrors of the DPO model cavity, or more general types of loss in the CIM experiment. The above equation is now studied through its equivalent positive-P phase-space representation [5]. This represents the density matrix through an exact expansion in terms of general off-diagonal coherent-state projectors,

$$\rho = \int P(\boldsymbol{\alpha}, \boldsymbol{\beta}) \frac{|\boldsymbol{\alpha}\rangle\langle\boldsymbol{\beta}^*|}{\langle\boldsymbol{\beta}^*|\boldsymbol{\alpha}\rangle} d^2\boldsymbol{\alpha} d^2\boldsymbol{\beta}\,. \quad (3.6)$$

The positive-P representation is chosen here over other representations first because it is strictly non-negative, has a probabilistic interpretation, and exists for all quantum states. It also results in a second-order Fokker-Planck equation (FPE) with positive-definite diffusion that has a corresponding stochastic process. This is achieved without the necessity to remove (truncate) higher-order derivative terms, which is important because equations with higher-order derivatives do not have a stochastic equivalent.

Mapping Eq. (3.5) to the positive-P representation using standard operator identities [6] yields

$$\begin{aligned}\frac{dP}{dt} = \Bigg\{ & \gamma_p\left(\frac{\partial}{\partial\alpha_p}\alpha_p + \frac{\partial}{\partial\beta_p}\beta_p\right) + \gamma_s\left(\frac{\partial}{\partial\alpha_s}\alpha_s + \frac{\partial}{\partial\beta_s}\beta_s\right) \\ & - \kappa\frac{\partial}{\partial\alpha_s}(\alpha_s\beta_p) - \kappa\frac{\partial}{\partial\beta_s}(\beta_p\alpha_s) \\ & + \frac{\partial}{\partial\alpha_p}\left(\frac{\kappa}{2}\alpha_s^2 - \mathcal{E}_p\right) + \frac{\partial}{\partial\beta_p}\left(\frac{\kappa}{2}\beta_s^2 - \mathcal{E}_p\right) \\ & + \frac{\kappa}{2}\left[\frac{\partial^2}{\partial\alpha_s^2}\alpha_p + \frac{\partial^2}{\partial\beta_s^2}\beta_p\right]\Bigg\} P, \end{aligned} \quad (3.7)$$

where $\boldsymbol{\alpha} \equiv (\alpha_s, \alpha_p)$ and similarly for $\boldsymbol{\beta}$.

Although this equation has a diffusion term which is not positive definite, the nonorthogonal nature of the coherent-state expansion allows one to obtain an equivalent, positive-definite FPE, which can then be mapped into equivalent stochastic equations. Equation (3.7) can be expressed through its corresponding set of stochastic differential equations (SDEs), which are

$$\begin{aligned}\frac{d}{dt}\alpha_s &= (-\gamma_s\alpha_s + \kappa\alpha_p\beta_s) + \sqrt{\kappa\alpha_p}\xi_1, \\ \frac{d}{dt}\beta_s &= (-\gamma_s\beta_s + \kappa\alpha_s\beta_p) + \sqrt{\kappa\beta_p}\xi_2, \\ \frac{d}{dt}\alpha_p &= \mathcal{E}_p - \gamma_p\alpha_p - \frac{\kappa}{2}\alpha_s^2, \\ \frac{d}{dt}\beta_p &= \mathcal{E}_p - \gamma_p\beta_p - \frac{\kappa}{2}\beta_s^2\,. \end{aligned} \quad (3.8)$$

The equations at this stage can be interpreted as either Stratonovich or Itô SDEs, since there is no difference between the main two types of stochastic calculus [48] for these equations. The terms ξ_1 and ξ_2 are independent delta-correlated Gaussian noises, so that

$$\langle\xi_i(t)\xi_j(t')\rangle = \delta_{ij}\delta(t-t'). \quad (3.9)$$

Usually, the pump field decay rate is much higher than the signal field decay rate, which merits the adiabatic approximation that $\frac{d}{dt}\alpha_p = \frac{d}{dt}\beta_p = 0$. Assuming this, and defining $\chi(\alpha) = \frac{\kappa\mathcal{E}_p}{\gamma_p} - \frac{\kappa^2}{2\gamma_p}\alpha^2$, the above SDEs reduce adiabatically [49] to a simpler Itô-type SDE:

$$\begin{aligned}\frac{d}{dt}\alpha_s &= (-\gamma_s\alpha_s + \chi(\alpha_s)\beta_s) + \sqrt{\chi(\alpha_s)}\xi_\alpha, \\ \frac{d}{dt}\beta_s &= (-\gamma_s\beta_s + \chi(\beta_s)\alpha_s) + \sqrt{\chi(\beta_s)}\xi_\beta\,. \end{aligned} \quad (3.10)$$

Based on this, one can reconstruct an adiabatic quantum master equation and find that

$$\frac{d\rho}{dt} = \frac{1}{i\hbar}[H_s, \rho] + \left[\gamma_s\mathcal{D}[a_s] + \frac{\kappa^2}{4\gamma_p}\mathcal{D}\left[a_s^2\right]\right]\rho, \quad (3.11)$$

where $H_s \equiv i\hbar\frac{\kappa\epsilon_p}{2\gamma_p}[(a_s^\dagger)^2 - a_s^2]$. It is also possible to carry out the adiabatic elimination from the master equation, giving an identical result [50].

The terms of Eqs. (3.10) illustrate the different physical processes happening simultaneously in the DPO cavity. The first term corresponds to linear decay, the second term to linear gain due to driving, and the third term to nonlinear gain saturation. The additional stochastic terms are due to quantum noise. However, individual trajectories do not necessarily correspond to individual experimental outcomes. From the expansion of Eq. (3.6), we see that averages over many trajectories are required to reconstruct even a single quantum state. Hence there is no general one-to-one correspondence between trajectories and experimental outcomes. Yet, due to the macroscopic nature of the ground state of the CIM, and the microscopic coherent state variance, we conjecture that one can regard the sign of the *final* coherent state output at any one site as giving the spin orientation at that site. This is confirmed, at least

for the current parameter values, by comparisons between the conditional and unconditional results for our simulations.

C. Relationship with neural networks

Before analyzing the CIM in a comprehensive, fully quantum physical description, we briefly want to point out its relation to neural networks. To do this, we take Eqs. (3.10) and make a number of modifications. These simplify the equations to a classical model, which takes us very far away from the world of quantum physics:

(a) We completely ignore the nondeterministic terms ξ_α, ξ_β. In other words, instead of a stochastic differential equation, we are looking at a completely deterministic ordinary differential equation.

(b) We assume that $\alpha = \beta$, thus reducing the DPO to a single equation of motion.

(c) We assume our phase-space variables are strictly real valued.

Further, we consider a set of N DPOs, corresponding to N spins in an Ising model. Additionally, each DPO experiences an additional term that drives the signal mode. This term corresponds to the signal injected by the optical delay lines or the feedback signal in the measurement-feedback architecture and is proportional to the interaction term in the Ising model Hamiltonian, via a proportionality factor ζ. For simplicity, we assume the external magnetic field (Zeeman term) to be zero.

Putting these assumptions together gives

$$\frac{d\alpha_i}{dt} = \zeta \sum_j J_{ij}\alpha_j + \left(\frac{\kappa \mathcal{E}_p}{\gamma_p} - \gamma_s\right)\alpha_i - \frac{\kappa^2 \alpha_i^3}{2\gamma_p}. \quad (3.12)$$

Let us compare the above equation with the concept of a neural network. A neural network broadly speaking consists of the following ingredients [51,52]:

(1) The first is a number of units, sometimes referred to as "cells," carrying a real value. These units can be arranged in multiple layers, in which case the network is referred to as a deep neural network, though other arrangements are possible as well.

(2) The second is a connection between the units across different layers or units in general.

(3) The thrid is a nonlinear output function associated with each unit. Though this might seem like an optional detail, it is actually a crucial component. Without nonlinearities, the network would be reduced to a linear function of its input values, regardless of its number of layers and internal complexity.

We can recognize all of these ingredients in Eq. (3.12). The variables α_i take the place of the network units. The $\sum_j J_{ij}\alpha_j$ term represents the connection between units while the remaining terms represent a third-order nonlinearity. Since there are no layers here and the units are connected to each other, Eq. (3.12) is most akin to a recurrent neural network (RNN) architecture.

Equation (3.12), though it is an incomplete description of the system since it does not take into account the quantum nature of the coherent Ising machine, can nevertheless be a useful tool to analyze the convergence properties that can be expected.

Equation (3.12) follows the potential function

$$\phi(\alpha_i) = -\zeta \sum_{i,j} J_{ij}\alpha_i\alpha_j - \frac{1}{2}\left(\frac{\kappa \mathcal{E}_p}{\gamma_p} - \gamma_s\right)\sum_i \alpha_i^2 + \frac{\kappa^2}{8\gamma_p}\sum_i \alpha_i^4. \quad (3.13)$$

The exact shape of the energy landscape strongly depends on $\mathbf{J}$. The configuration that classically solves the Ising problem constitutes the energetic minimum; however, different configurations can (and typically do) manifest as local minima, which poses obstacles in determining the ground state. Stochasticity terms originating from quantum effects and from environment interactions will contribute to exploring the energy landscape. However, like a true Ising model, it is possible and quite probable for the system to evolve into a local minimum, which is not necessarily the global optimal minimum. The likelihood of this is not only determined by the Ising problem itself, but also by the minimization strategy that is employed.

A simple minimization strategy consists in linearly ramping up the pump rate $\mathcal{E}_p$. Similar to the single DPO, which experiences a bifurcation when $\mathcal{E}_p$ reaches $\mathcal{E}_{p,th}$, minima in the energy landscape in Eq. (3.13) will appear or become more pronounced with higher $\mathcal{E}_p$. In comparison to a single DPO, the pump strength at which local minima appear is usually lower for a network of coupled DPOs. For a more gradual increase in $\mathcal{E}_p$, the local minima appear more slowly which makes the minimization a more adiabatic one, which in turn increases the likelihood of finding the global minimum for the price of an overall longer simulation time. Once a certain pump strength is reached, the system experiences a so-called freeze-out, from which the spin states do not change any more. This effectively marks the end of the simulation process.

Besides this simple strategy, more sophisticated ones exist as well, which can result in a higher likelihood of reaching the ground state.

IV. QUANTUM FEEDBACK CIM

A. Measurement-feedback theory

The framework of measurement-feedback systems was developed in the early 1990s [53–58] and is based on earlier theories of measurement [59]. We will review the basic concepts first before applying them to the CIM.

We start by considering a quantum system described by the density matrix ρ subject to the evolution

$$\frac{d}{dt}\rho(t) = \mathcal{L}\rho(t), \quad (4.1)$$

where $\mathcal{L}$ includes both unitary and nonunitary terms.

B. Quantum stochastic measurement equations

Next, suppose that a continuous quantum measurement of an Hermitian operator $c + c^\dagger$ is carried out, which in this case is the output field proportional to the quadrature $\hat{X} = a + a^\dagger$. The measurement outcome at time t is determined not only by the state $\rho(t)$, but also by the quantum noise that is introduced in the measurement process and cannot be eliminated by an

improved measurement apparatus. The system state $\rho(t)$ partially collapses based on the measurement outcome. Because the measurement outcome is not predictable, due to quantum noise, the state of ρ at time $t + dt$ is not predictable either.

The measurement outcome and the evolution of ρ become intertwined. To make this problem more tractable, one introduces the *conditional* state $\rho_c(t)$ and measurement outcome $I_c(t)$. Here, conditional refers to a specific *realization* of the quantum measurement noise. As well as generating a directly measured outcome, the measurement changes the quantum state, in a process described by the generalized theory of measurement effects and operations [59,60].

Assuming a detector with perfect efficiency is used, these are obtained in this case [54] as

$$\frac{d}{dt}\rho_c(t) = [\mathcal{L} + \xi(t)\mathcal{H}[c]]\rho_c(t)\,. \tag{4.2}$$

Here $\xi(t)$ is the fluctuating part of the feedback current:

$$I_c(t) = \langle c + c^\dagger\rangle_c(t) + \xi(t), \tag{4.3}$$

while $\langle c + c^\dagger\rangle_c(t) \equiv \mathrm{Tr}[(c + c^\dagger)\rho_c(t)]$, and $\xi(t)$ is a Gaussian delta-correlated noise as in Eq. (3.9). The superoperator $\mathcal{H}[\cdot]$, which describes the effects of the measurement and ensures preservation of the trace of ρ_c, is called the innovation operator, and is defined as

$$\mathcal{H}[c]\rho \equiv c\rho + \rho c^\dagger - \mathrm{Tr}[c\rho + \rho c^\dagger]\rho\,. \tag{4.4}$$

The term $\xi(t)$ represents the quantum measurement noise. Equation (4.2) is to be understood as an Itô-type SDE, but with operator rather than c-number stochastic variables.

C. Itô and Stratonovich equations

For use in simulating conditional feedback, we will use the equivalent Stratonovich master equation. These have the advantage that they satisfy the standard rules of calculus, and are generally simpler to integrate. The theory of this equivalence is well understood [48]. A generic multivariate, m-dimensional Markovian stochastic process has an Itô-type equation

$$\frac{d}{dt}\mathbf{X}^{(I)} = \mathbf{A}(\mathbf{X}) + \mathbf{B}(\mathbf{X})\boldsymbol{\xi}(t)\,, \tag{4.5}$$

where $\mathbf{A}$ is an m-dimensional vector, $\mathbf{B}$ is an $(m \times n)$-dimensional matrix, and $\boldsymbol{\xi}$ is an n-dimensional noise correlated according to Eq. (3.9). The corresponding Stratonovich-type stochastic differential equation can be found via

$$\frac{d}{dt}\mathbf{X}^{(S)} = \mathbf{A}(\mathbf{X}) + \mathbf{C}(\mathbf{X}) + \mathbf{B}(\mathbf{X})\boldsymbol{\xi}(t)\,. \tag{4.6}$$

Here, $\mathbf{C}(\mathbf{X})$ is called the Stratonovich correction term, where

$$C_i(\mathbf{X}) = -\frac{1}{2}\sum_{k,j}\frac{\partial B_{ik}}{\partial X_j}(\mathbf{X})B_{jk}(\mathbf{X}). \tag{4.7}$$

For complex stochastic vectors, one can generalize this by expanding in real and imaginary parts or by using Wirtinger calculus. Although Eq. (4.2) is an operator equation, the above transformation rule can be applied by considering the quantum operators, including the density operator, as large matrices. This way, one finds a Stratonovich correction term as in Eq. (4.6).

Hence, for complex stochastic matrices X_{ij}, if $\mu = (i, j)$ and $\nu = (i', j')$, one obtains

$$C_\mu = -\frac{1}{2}\sum_{k,\nu}\left[B_{\nu k}\frac{\partial}{\partial X_\nu} + B^*_{\nu k}\frac{\partial}{\partial X^*_\nu}\right]B_{\mu k}\,. \tag{4.8}$$

In the cases treated here, since $\mathcal{H}[c]\rho_c$ is analytic in ρ, there is no extra Wirtinger term from the conjugate derivative. The resulting Stratonovich correction corresponding to the single-mode measurement operator $\mathcal{H}[c]\rho$ is

$$C^{\mathcal{H}}[c]\rho_c = \langle c + c^\dagger\rangle_c\mathcal{H}[c]\rho_c - \tfrac{1}{2}\mathcal{H}[c^2]\rho_c + \langle c^\dagger c\rangle\rho_c - c\rho_c c^\dagger. \tag{4.9}$$

Although reported previously [61], this result is not well known, and we give the complete proof in the Appendix. Hence, the equivalent Stratonovich-type master equation is therefore obtained as

$$\frac{d}{dt}\rho_c = [\mathcal{L} + \xi(t)\mathcal{H}[c] + C^{\mathcal{H}}]\rho_c(t)\,. \tag{4.10}$$

For our purposes, the operator c is proportional to the operator a of the DPO signal state, which corresponds to homodyne detection. It is important to note that since a measurement of c is taking place, there needs to be a loss term $\mathcal{D}[c]$ included in the operator $\mathcal{L}$. For example, if a homodyne detection is being carried out, the operator $\mathcal{D}[a]$ is required to account for the fact that part of the signal leaves the cavity for the detector.

Realistically, the detector will have limited detection efficiency. This can be accounted for by "splitting up" the fraction of the signal which enters the detector into a fraction which decays without being detected and a fraction which decays while being detected. This will be demonstrated shortly when the measurement-feedback scheme is applied to the CIM.

D. Feedback master equations

We now wish extend the system so that it includes a feedback which is applied to ρ_c based on the measurement $I_c(t)$. The feedback is expressed by a superoperator $\mathcal{K}$ which depends on the feedback mechanism. This may be defined as a unitary operator via $\mathcal{K}\rho \equiv [K, \rho]$, where K is an arbitrary operator. We further limit ourselves to the case where the feedback superoperator is a linear function of the measurement result $I_c(t)$.

Between the measurement of the system state and the application of feedback, there is always some delay time τ. For example, in the case of our MFB CIM, there is the propagation time between the photodetector, the FPGA, and the signal generator as well as the calculation time of the FPGA. Hence, in a precise description, the feedback operator would be proportional to a retarded measurement operator, i.e., $I_c(t - \tau)\mathcal{K}\rho(t)$. To simplify things, we want to take the limit of $\tau \to 0$.

A naive approach to incorporate the feedback would then be simply to add a feedback term $I_c(t)\mathcal{K}\rho_c(t)$ to Eq. (4.2) to get

$$\frac{d}{dt}\rho_c(t) = [\mathcal{L} + \xi(t)\mathcal{H}[c] + I_c(t)\mathcal{K}]\rho_c(t)\,. \tag{4.11}$$

However, this approach poses a conceptual problem, and this equation will not be used. Even in the limit $\tau \to 0$, any feedback based on a specific measurement happens *after* the state collapse of the wave function in relation to this measurement outcome. When formulating Eq. (4.11), we have not done anything to take this causal delay into account.

In fact, with the definition of $I_c(t)$, Eq. (4.11) indicates that the wave-function collapse happens simultaneously with the feedback. In the following sections, we describe the theory that solves this problem.

The correct expression for the feedback equation can be found following a derivation in [53]. Here, the action of the feedback is accounted for via an exponential term that acts from the left on the remaining terms. This ensures the correct operator ordering between $\mathcal{K}$ and $\mathcal{H}$, consistent with the fact that feedback necessarily follows after the wave-function collapse or measurement process.

We describe the general approach here, and use it to obtain a conditional master equation for one mode, which will be generalized in the next section. We use the definition of $I_c(t)$ and express the feedback as well as Eq. (4.1) in differential form to get

$$\rho_c(t+dt) = \exp[\langle c + c^\dagger\rangle_c(t)\mathcal{K}\cdot dt + \mathcal{K}\cdot dW] \times[1 + (\mathcal{L}\cdot dt + dW\cdot\mathcal{H}[c])]\rho_c(t), \quad (4.12)$$

where dW is the noise increment of $\xi(t)$ in time dt, that is, $\xi(t) = dW/dt$.

One now expands the exponential in Eq. (4.12) to second order, expands the product, and disregards terms of order $O(dt^{3/2})$ and above. We use the prescription that $dW^2 \sim dt$. The approach given here omits details that are given in the original literature [54,62]. This leads to an Itô equation,

$$\begin{aligned}\frac{d}{dt}\rho_c(t) &= \frac{1}{dt}[\rho_c(t+dt) - \rho_c(t)] \\ &= \mathcal{L}\rho_c(t) + \mathcal{K}(c\rho_c(t) + \rho_c(t)c^\dagger) \\ &\quad + \left\{\frac{1}{2}\mathcal{K}^2 + \xi(t)[\mathcal{H}[c] + \mathcal{K}]\right\}\rho_c(t). \quad (4.13)\end{aligned}$$

Like Eq. (4.2), Eq. (4.13) is an Itô-type stochastic differential equation. As an alternative approach of obtaining Eq. (4.13), Eq. (4.2) can be transformed into its corresponding Stratonovich form. Following the procedure described in the Appendix, which takes account of all the Stratonovich corrections, one obtains under certain restrictions for the form of the superoperators $\mathcal{H}$ and $\mathcal{K}$ that

$$\frac{d}{dt}\rho_c^{(S)} = \left[\mathcal{L} + \langle c^\dagger c\rangle - \frac{1}{2}\mathcal{H}[cc] + I_c(\mathcal{H}[c] + \mathcal{K})\right]\rho_c - c\rho_c c^\dagger, \quad (4.14)$$

where $I_c(t)$ is given by Eq. (4.3).

Equations (4.13) and (4.14) describe the evolution of the system for a given measurement noise outcome $\xi(t)$. However, in many cases we are not interested in what happens for a specific noise realization, but rather what happens over a range of many noise realizations. In such cases we can average the Itô master equation over the infinitely many outcomes for $\xi(t)$ to obtain $\langle \frac{d}{dt}\rho_c(t)\rangle_{\xi(t)} = \frac{d}{dt}\langle\rho_c(t)\rangle_{\xi(t)}$.

Defining $\rho \equiv \langle\rho_c(t)\rangle_{\xi(t)}$, the average over this type of Itô stochastic equation has the effect of simply removing the noise terms, due to linearity and the nonanticipating nature of Itô calculus [48]. Therefore, this yields a much simpler equation:

$$\frac{d}{dt}\rho = \mathcal{L}\rho + \mathcal{K}(c\rho + \rho c^\dagger) + \frac{1}{2}\mathcal{K}^2\rho\,. \quad (4.15)$$

E. Master equation for multiple nodes

We now consider a CIM with N DPOs (spin states). We assume the adiabatic approximation and label the spin states $a_1, \ldots, a_N$, dropping the index s. The right-hand side (RHS) of Eq. (3.11), applied to all modes a_i, is equivalent to $\mathcal{L}\rho(t)$ in the framework outlined above. We now introduce a second channel through which the signal decays with rate γ_m. The fraction of the signal that decays through this channel is observed by a homodyne detector with perfect efficiency. This way, a homodyne detector with limited efficiency can be described by declaring that the fraction not picked up by the detector decays through the channel already present in Eq. (3.11). Thus, we have to add another set of diffusive terms $\gamma_m\mathcal{D}[a_i]$.

With $\gamma \equiv \gamma_s + \gamma_m$, these can be combined to yield $\gamma\mathcal{D}[a_i]$. The operator subject to the innovation operator $\mathcal{H}[\cdot]$ is $\sqrt{2\gamma_m}a_i$. Thus, *without* the feedback, we obtain the total master equation

$$\begin{aligned}\frac{d}{dt}\rho &= \frac{1}{i\hbar}[H_s, \rho] + \sum_i\left\{\gamma\mathcal{D}[a_i]\rho + \frac{\kappa^2}{4\gamma_p}\mathcal{D}\big[a_i^2\big]\rho\right\}\rho \\ &\quad + \sum_i \mathcal{H}\big[\sqrt{2\gamma}a_i\big]\rho \\ &\equiv \mathcal{L}\rho + \sum_i \mathcal{H}\big[\sqrt{2\gamma}a_i\big]\rho\,, \quad (4.16)\end{aligned}$$

where

$$H_s = i\hbar\frac{\kappa\epsilon_p}{2\gamma_p}\sum_i\big[(a_i^\dagger)^2 - a_i^2\big]. \quad (4.17)$$

This treats many modes in parallel, with measurement as well, but there is no feedback included at this stage.

We now extend the framework outlined so far to include several modes *including* feedback. The interaction matrix $\mathbf{J}$ is typically denser than a permutation matrix; in other words, a measurement outcome for one mode a_i will generally produce feedback in several modes among $a_1, \ldots, a_N$ proportional to $J_{i1}, \ldots, J_{iN}$. As a result, Eq. (4.12) becomes

$$\rho_c(t+dt) = \exp\left[\sum_i \mathcal{K}_i\sum_j J_{ij}[\langle c_j + c_j^\dagger\rangle_c dt + dW_j]\right] \times\left[\rho_c + \left(\mathcal{L}\cdot dt + \sum_j dW_j\cdot\mathcal{H}[c_j]\right)\rho_c\right], \quad (4.18)$$

where time-dependent functions on the RHS are evaluated at (t), and $\mathcal{K}_i$ is the superoperator that generates feedback for the ith mode.

After expanding Eq. (4.18) and retaining all terms of order $O(dt)$, $O(dW)$, and $O(1)$, one finds

$$\frac{d}{dt}\rho_c = \mathcal{L}\rho_c + \sum_{ij}\mathcal{K}_i[J_{ij}(c_j\rho_c+\rho_c c_j^\dagger)]+\frac{1}{2}\sum_{i,j,k}J_{ij}J_{ik}\mathcal{K}_i\mathcal{K}_k\rho_c + \sum_i \xi_i(t)\left[\mathcal{H}[c_i]+\sum_j J_{ij}\mathcal{K}_j\right]\rho_c\,. \tag{4.19}$$

This is an Itô conditional master equation, which needs to be solved relative to every noise realization. Consider a single entry J_{ij} from the interaction matrix $\mathbf{J}$. We want the feedback to induce the signal $\zeta J_{ij}(a_j\rho+\rho a_j^\dagger)$ into the ith mode. With the definition of $c_j=\sqrt{2\gamma_m}a_j$, we find that

$$\mathcal{K}_i\rho = \frac{\zeta}{\sqrt{2\gamma_m}}[a_i^\dagger - a_i,\rho]\,. \tag{4.20}$$

Using the techniques from Sec. IV D, the Stratonovich form of Eq. (4.19) is found to be

$$\frac{d}{dt}\rho_c^{(S)} = \mathcal{L}\rho_c^{(S)} + \sum_{ij}\mathcal{K}_iJ_{ij}\langle c_j+c_j^\dagger\rangle + \sum_i\xi_i(t)\left[\mathcal{H}[c_i]+\sum_j J_{ij}\mathcal{K}_j\right]\rho_c^{(S)} + \sum_i C^{\mathcal{H}}[c_i]\rho_c^{(S)} \tag{4.21}$$

with $C^{\mathcal{H}}$ given in Eq. (4.9).

For the Itô form, given in Eq. (4.19), averaging over the noise outcomes simply removes the last term in Eq. (4.19), and yields

$$\frac{d}{dt}\rho = \mathcal{L}\rho + \sum_i\mathcal{K}_i\sum_j J_{ij}(c_j\rho+\rho c_j^\dagger)(t) + \frac{1}{2}\sum_{i,j,k}J_{ij}J_{ik}\mathcal{K}_i\mathcal{K}_k\rho\,. \tag{4.22}$$

Finally, we have all ingredients for a full description of the MFB-type CIM. Substituting all definitions, we get the total quantum master equation

$$\frac{d\rho}{dt} = \sum_i\left(\frac{\kappa\epsilon_{pi}}{2\gamma_p}\left[(a_i^\dagger)^2-a_i^2,\rho\right]+\gamma\mathcal{D}[a_i]\rho + \frac{\kappa^2}{4\gamma_p}\mathcal{D}\left[a_i^2\right]\rho+\zeta\sum_j J_{ij}[a_i^\dagger-a_i,a_j\rho+\rho a_j^\dagger] + \frac{\zeta^2}{4\gamma_m}\sum_{j,k}J_{ij}J_{ik}[a_i^\dagger-a_i,[a_k^\dagger-a_k,\rho]]\right). \tag{4.23}$$

Such total master equations have been numerically solved then compared to experiment in much simpler cases of laser cooling through feedback [63]. In these studies, comparison to the full conditional master equation was generally not carried out, due to the computational and experimental complexity of recording and storing the full measurement history for each feedback realization.

F. Total phase-space simulations

Even though very much simpler than the conditional master equation, the total master equation, Eq. (4.23), is still insoluble analytically, as far as we know. Treating it with orthogonal state expansions is exponentially hard with large numbers of modes, as in the CIM. It has only been carried out for small Hilbert spaces, usually involving state truncation as well [63].

Despite this, it can be simulated via phase-space methods, using the positive-P representation. This solves the exponential hardness problem through probabilistic sampling. These techniques are known to be successful in a number of similar cases with large bosonic Hilbert spaces [47]. There is a known limitation, however. For low losses, high nonlinearities, and long time evolution, boundary term errors can break the stochastic equivalence [7,9]. While this can be treated using stochastic gauge methods [64], this is not required for typical CIM parameters.

Using the standard rules, Eq. (4.23) translates to the Fokker-Planck equation

$$\frac{dP}{dt} = \Bigg\{\sum_i\left[\partial_{\alpha_i}(\gamma\alpha_i-\chi(\alpha_i)\beta_i)+\partial_{\alpha_i}^2\chi(\alpha_i)\right] + \sum_i\left[\partial_{\beta_i}(\gamma\beta_i-\chi(\beta_i)\alpha_i)+\partial_\beta^2\chi(\beta_i)\right] + f^2\sum_{i,j,k}J_{ij}J_{ik}(\partial_{\alpha_i}+\partial_{\beta_i})(\partial_{\alpha_k}+\partial_{\beta_k}) - \sum_{i,j}(\partial_{\alpha_i}+\partial_{\beta_i})\zeta J_{ij}(\alpha_j+\beta_j)\Bigg\}P\,, \tag{4.24}$$

where $f=\zeta/\sqrt{2\gamma_m}$, and $P\equiv P(\alpha_1,\beta_1,\ldots,\alpha_N,\beta_N)$.

Translating this to a set of stochastic differential equations yields

$$\dot{\alpha}_i = [\epsilon_i-\gamma\alpha_i+\beta_i\chi(\alpha_i)]+\sqrt{\chi(\alpha_i)}\xi_i^\alpha+f\sum_j J_{ij}\xi_j,$$
$$\dot{\beta}_i = [\epsilon_i-\gamma\beta_i+\alpha_i\chi(\beta_i)]+\sqrt{\chi(\beta_i)}\xi_i^\beta+f\sum_j J_{ij}\xi_j, \tag{4.25}$$

with the definitions that

$$\chi(\alpha)\equiv\frac{\kappa}{\gamma_p}\left[\epsilon_p-\frac{\kappa}{2}\alpha^2\right],$$
$$\epsilon_i = \zeta\sum_j J_{ij}(\alpha_j+\beta_j)\,. \tag{4.26}$$

The equations above are also Itô stochastic equations, although the noise terms correspond to the total quantum noise in the system itself. Stratonovich equations, which are more tractable numerically, are then obtained by the mapping of $\gamma\to\gamma'\equiv\gamma-\kappa^2/4\gamma_p$ [6]. This allows one to use more robust and accurate numerical techniques [65].

G. Conditional phase-space simulations

In Eq. (4.25), the measurement noise has been averaged over, thus removing it from the equations. Because of this, it allows for a very efficient numerical simulation of the CIM. In addition to the total master equation given by Eq. (4.23), we would also like to simulate the conditional master equation with the measurement noise present. We expect that simulating the conditional master equation for different realizations of the measurement noise and averaging the simulation outcome will produce results consistent with those obtained from the total master equation.

While a conditional master equation approach is not the most efficient one, there are nevertheless good reasons to pursue it. For one, it allows us to carry out a consistency check between the conditional and total master equations. At the same time, there might be situations where (at least partial) knowledge of the measurement noise exists, for example when the measurement outcome is recorded. Furthermore, there are cases for which a total master equation might not be found as easily. One such case is where the finite time delay is to be taken into account explicitly. In a phase-space simulation, this could mean applying feedback based on the system state and measurement noise from one or more time steps ago. Also, a total master equation may not be found as easily if the feedback is not strictly proportional to the measurement outcome.

In our derivation of the total master equation, we have made the assumption that the feedback is proportional to the measurement outcome immediately after the collapse of the wave function. This enabled us to find Eq. (4.19), where terms of second order in ρ_c (through the trace operator included in $\mathcal{H}$) only appear multiplied with the measurement noise. By averaging over measurement noises, we removed this term and obtained a fully deterministic master equation which is strictly linear in ρ. If the feedback is not proportional to the measurement outcome $I_s(t)$, averaging over the measurement noise would most likely result in a master equation with higher-order terms in ρ (through the trace operator), which is forbidden [66].

We now attempt to formulate a set of phase-space equations with which to simulate the conditional master equation. The most obvious approach would be to apply the familiar chain of transformations "quantum master equation → Fokker-Planck equation → stochastic differential equations" to Eq. (4.19) as we did for Eq. (4.23). However, there are several problems with Eq. (4.19) when it comes to finding a corresponding Fokker-Planck equation: First, there is a noise term $\xi(t)$, which means the master equation itself is a stochastic equation. A Fokker-Planck equation is a deterministic partial differential equation. Furthermore, a Fokker-Planck equation has only first- and second-order derivative terms with respect to its phase-space variables. Equation (4.19) would clearly lead to nonderivative terms due to the operator $\mathcal{H}[c_i]$. Lastly, due to the expectation value in $\mathcal{H}[c_i]$, the corresponding equation describing the phase-space distribution would result in an integro-differential equation, another difference from a conventional Fokker-Planck equation.

Hush *et al.* [10] investigated the question how a Fokker-Planck-like equation with these features can be simulated efficiently using stochastic samples. They consider a general equation of the form

$$dP = \left\{\left(-\sum_i \partial_i A_i + \frac{1}{2}\sum_{i,j}\partial_i C_{ij}\partial_{i'}C_{i'k} + \iota - \langle\iota\rangle\right)dt + \sum_j\left(-\sum_i \partial_i B_{ij} + \nu_j - \langle\nu_j\rangle\right)dW_j^{(s)}\right\}P, \quad (4.27)$$

where $P \equiv P(\mathbf{x}, \mathbf{dW}^{(s)}(t), t)$, while $\mathbf{x}$ and $\mathbf{dW}^{(s)}$ are vectors of (phase-space) variables and noise increments, respectively. The terms A, B, C, ι, and ν are (vector-, matrix-, and scalar-valued) functions which may depend on $\mathbf{x}$ as well as the distribution P. Unlike the stochastic equations we have considered so far, Eq. (4.27) is understood to be in the Stratonovich calculus, indicated by the superscript (s).

Hush *et al.* demonstrated that Eq. (4.27) can be treated using a set of Stratonovich-type stochastic differential equations with the addition of a weight variable $\omega(t)$. The full set of stochastic equations is

$$dx_i = A_i dt + \sum_j B_{ij}(x,t)dW_j^{(s)} + \sum_k C_{ik}(x,t)dV_k^{(s)}, \quad (4.28)$$

$$\frac{d\omega}{\omega} = \iota(x,t)dt + \sum_j \nu_j(x,t)dW_j^{(s)}, \quad (4.29)$$

where both $dW^{(s)} = dW^{(s)}(t)$ and $dV^{(s)} = dV^{(s)}(t)$ are Stratonovich-type noise increments. However, there is a profound difference between these two noise terms. The dV terms originate from second-order derivatives in Eq. (4.27) just like for a conventional Fokker-Planck equation. As such, they are independently drawn for every stochastic sample that is simulated. In contrast, the dW terms correspond to the measurement noise in Eq. (4.27) and are drawn once per time step for the entire stochastic ensemble. Due to the nature of the dV terms, they are called "fictitious" noises, while the dW terms are called "real" noises.

Any observables $f(\mathbf{x})$ based on the conditional equations are obtained via

$$\overline{f(\mathbf{x})} \equiv \mathbb{E}[\omega f(\mathbf{x})]/\mathbb{E}[\omega]\,. \quad (4.30)$$

Here $\mathbb{E}[\cdot]$ indicates the average with respect to stochastic trajectories.

While the above method in principle will provide the correct predictions, it is obvious from Eq. (4.29) that the noises are likely to cause numerical instabilities due exponential decay and growth. In order to make the simulations more tractable, there are three additions that can be made to the conventional Monte Carlo simulation algorithm of Eqs. (4.28) and (4.29).

The first and most important addition is a technique called breeding. Its purpose is to "even out" the distribution of weights by cloning the highest-weighted trajectories into two copies with half their original weight while simultaneously removing trajectories with extremely low weight. More precisely, the breeding algorithm consists of the following steps:

(1) Find the trajectory index i with lowest weight $\omega_{\min}$. Calculate the ratio r between lowest weight and average weight $r \leftarrow \omega_{\min}/\langle\omega\rangle$. If r is less than a cutoff ratio $\epsilon_{\text{thr,breed}}$,

continue with the next steps. Otherwise, do nothing (terminate).

(2) Find the trajectory index j with highest height $\omega_{\max}$. Replace the ith trajectory by jth trajectory, i.e., $\mathbf{x}_i \leftarrow \mathbf{x}_j$. Set the weights of both trajectories to half of $\omega_{\max}$, i.e., $\omega_i \leftarrow \omega_{\max}/2$, $\omega_j \leftarrow \omega_{\max}/2$.

(3) Go back to step 1.

We have found that the breeding algorithm works best when executed after every time step in the stochastic integration. When running the stochastic integration, we are recording the number of "breed" events, that is, the number of times step 2 is executed.

Another addition which improves numerical stability is to normalize the weights, i.e., $\omega \leftarrow \omega/\langle\omega\rangle$. In our simulations, this is done following the breeding algorithm.

Lastly, instead of simulating the weights ω themselves, we are using the transformed weights $\omega' = \log(\omega)$. This leads to a differential equation for the transformed weights:

$$d\omega' = \iota(x(t),t)dt + \sum_j \nu_j(x(t),t)dW_j^{(s)}(t). \quad (4.31)$$

In order to apply the above method to the coherent Ising machine, it is necessary to reconsider the issue of feedback, the reason being that Eq. (4.27) is a Stratonovich-type stochastic equation, whereas so far we have treated measurement-feedback systems entirely in the Itô scheme. Note that for measurement-feedback systems, the choice of integration scheme has a subtle effect on the interpretation of the feedback noise as will be shown shortly.

After mapping the Stratonovich-type master equation given in Eq. (4.21) to the positive-P representation, which results in a Fokker-Planck-like equation, one can apply the weighted integration scheme. This results in the Stratonovich-type stochastic differential equations

$$\begin{aligned}
\dot{\alpha}_i &= \left[\epsilon_i + \left(\frac{\kappa^2}{4\gamma_p} - \gamma\right)\alpha_i^2 + \beta_i\chi(\alpha_i)\right] + \sqrt{\chi(\alpha_i)}\xi_i^{\alpha},\\
\dot{\beta}_i &= \left[\epsilon_i + \left(\frac{\kappa^2}{4\gamma_p} - \gamma\right)\beta_i^2 + \alpha_i\chi(\beta_i)\right]dt + \sqrt{\chi(\beta_i)}\xi_i^{\beta},\\
\dot{\omega} &= \gamma_m \sum_i (\alpha_i+\beta_i)(2\langle\alpha_i+\beta_i\rangle - (\alpha_i+\beta_i))\\
&\quad + \sqrt{2\gamma_m}\sum_i (\alpha_i+\beta_i)\xi_i^r\,, \qquad (4.32)
\end{aligned}$$

where

$$\epsilon_i = \zeta \sum_j J_{ij}\left(\langle\alpha_j+\beta_j\rangle + \frac{\xi_i^r}{\sqrt{2\gamma_m}}\right). \quad (4.33)$$

Here, ξ_i^{α} and ξ_i^{β} correspond to "fictitious" noises while ξ_i^r correspond to measurement ("real") noises.

V. NUMERICAL RESULTS

Three different types of simulation were carried out to illustrate and compare the methods. While the coherent state expansion means that one can only rigorously compare the averages over many trajectories, in fact the method is even more powerful than this. Since the final state has a macroscopic distinction between "spin up" and "spin down," one can also compare the actual distributions of the final results, and this will correspond to the corresponding experimental distributions due to their macroscopicity.

A. Small-scale pump ramps

An experiment is considered with $N = 16$ degenerate parametric oscillators. The interaction matrix $\mathbf{J}$ corresponds to the one-dimensional (circular) antisymmetric Ising model, that is, $J_{ij} = -1$ if $|i-j| = 1$ or $|i-j| = N-1$, $J_{ij} = 0$ otherwise.

The system parameters are $\gamma_s = 1.0$, $\gamma_m = 0.1$, $\gamma_p = 10$, and $\kappa = 0.1$. $N_T = 500 \times 10^3$ time steps and $N_s = 8192$ stochastic samples were used for the integration.

The pump strength was linearly increased from $\varepsilon_p = 0$ to $\varepsilon_p = 2\varepsilon_{p,th}$ with $\varepsilon_{p,th} = \frac{\gamma\gamma_p}{\kappa}$, where $\gamma \equiv \gamma_s + \gamma_m$ during the integration time.

The integration was carried out for the total master equation as well as the conditional master equation with the weighted scheme explained previously using a stochastic RK4 integration scheme. For the weighted scheme, the weight rebalancing (breeding) algorithm was carried out after each time step using a breeding threshold of $\epsilon_{th} = 10^{-4}$.

The simulation was repeated for three different integration times and nine different values for the feedback parameter ζ.

A success rate is defined as the fraction of instances for which the simulated system ascertains the Ising model ground state. Here, the ground state is given by the degenerate states $(+,-,\ldots,+,-)$ and $(-,+,\ldots,-,+)$, where the spin states are given by the sign of the mode's x quadrature. In the case of the total master equation, the success rate can be calculated by considering all N_s individual trajectories. Here, 20 independent simulations with N_s trajectories were used to determine the error of the mean, which is negligibly small. For the case of the weighted simulations, this is considerably more resource intensive, demonstrating the clear superiority of the total master equation method. Here, the entire stochastic ensemble is needed to determine a mode's x quadrature according to Eq. (4.30). The experiment is repeated 200 times in order to determine the success probability. However, there are not enough data to determine the error of the mean. The results are shown in Fig. 4.

In the case of the total master equation for an interaction strength of $\zeta = 0.12$, the probability density for the Ising model Hamiltonian is recorded, which is defined as

$$\mathcal{H} = -\sum_{i,j} s_i(\mathbf{J}_{ij})s_j\,, \quad (5.1)$$

where s_i indicates the corresponding spin state given by the x quadrature of the ith DPO mode, that is,

$$s_i \equiv \mathrm{sgn}(\mathrm{Re}(\alpha_i+\beta_i))\,. \quad (5.2)$$

The probability density is shown in Fig. 5.

B. Small-scale pump and feedback ramps

A second experiment is considered with the system parameters given above. Here, a different minimization strategy is employed. Where in the first experiment, the pump strength was linearly increased during the simulation time, now the

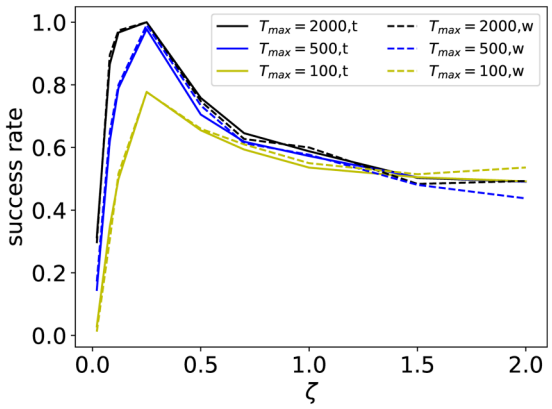

FIG. 4. Success probabilities for the CIM with $N = 16$ sites and linearly increased pump field, as a function of the (constant) feedback strength ζ for three different integration times. The results were obtained using the conditional (weighted) integration scheme (abbreviated with "w" in the legend) and the total master equation method (abbreviated with "t" in the legend).

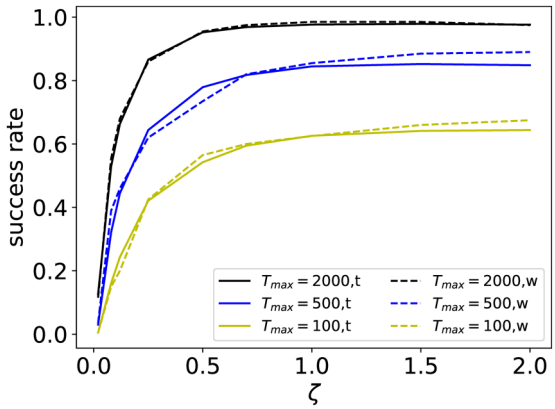

FIG. 6. Success probabilities for the CIM with $N = 16$ sites and linearly increased pump field and feedback strength, as a function of the maximum feedback strength $\zeta_{\max}$ for three different integration times. The results were obtained using both the conditional (weighted) integration scheme (abbreviated with "w" in the legend) and the total master equation method (abbreviated with "t" in the legend).

pump strength as well as the feedback parameter ζ are linearly increased to $2\varepsilon_{p,th}$ and $\zeta = \zeta_{\max}$, respectively. As with the first experiment, 20 independent simulations were used in the case of the total master equation simulations to estimate the error of the mean, while 200 independent repetitions were used to estimate the success probability in the case of the conditional (weighted) method. This is shown in Fig. 6.

We note the greatly improved success rate at large feedback strengths, indicating the sensitivity of the CIM to different ramp strategies. As before, there is excellent agreement between the conditional and unconditional methods.

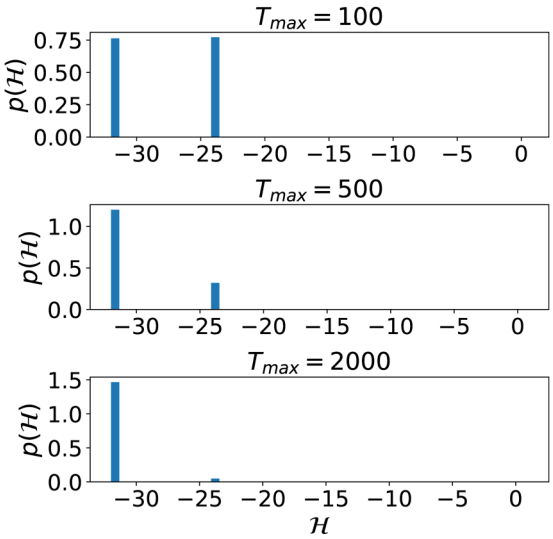

FIG. 5. Probability density of the Ising model Hamiltonian for the CIM with $N = 16$ sites and linearly increased pump field with a constant feedback strength of $\zeta = 0.12$ for three different integration times. The results were obtained using the total master equation method and are based on 6144 stochastic trajectories.

C. Large-scale pump ramps

Lastly, we consider an experiment consisting of $N = 1000$ parametric oscillators, using a linear pump ramp. Due to its large size, only the much faster unconditional simulations were run.

As outlined in Sec. II A, an Ising model can be identified with a (weighted, undirected) graph with the interaction matrix $\mathbf{J}$ corresponding to the adjacency matrix and weight function, respectively. Here, the interaction matrix is chosen so that it corresponds to a random graph generated using the following set of rules:

(i) Each of the $\frac{N(N-1)}{2}$ edges has nonzero weight with a probability of p and zero weight with a probability of $1 - p$. Here, $p = 0.1$.

(ii) A nonzero weight is either $+1$ or -1 with equal probability.

In other words, $\mathbf{J}$ is a symmetric 1000×1000 matrix with main diagonal entries equal to zero off-diagonal entries equal to zero with probability $1 - p$, $+1$ with probability $\frac{p}{2}$, and -1 with probability $\frac{p}{2}$.

The interaction matrix is generated once and used for all quantum trajectories of the stochastic simulation.

The system parameters are $\gamma_s = 1.0$, $\gamma_m = 0.1$, $\gamma_p = 10$, $\kappa = 0.1$, $N_T = 10 \times 10^3$, $\zeta = 0.1$, and $T_{\max} = 10$. The pump strength is linearly increased from $\varepsilon_p = 0$ to $\varepsilon_p = 3\varepsilon_{p,th}$ during the integration time. Due to the exponential complexity of the problem, precise knowledge of the ground state of the system considered here is likely impossible. Hence, instead of the success probability for finding the ground state, the Ising model interaction Hamiltonian is considered.

The simulation was carried out using a total of $N_S = 102\,400$ stochastic trajectories with interaction strength of $\zeta = 0.05$. They took about 12 hours on 40 state-of-the-art GPUs running in parallel on a computer cluster. The resulting probability density for a given outcome of the interaction energy is given in Fig. 7, while Fig. 8 shows the evolution of the mean interaction energy as a function of simulation time.

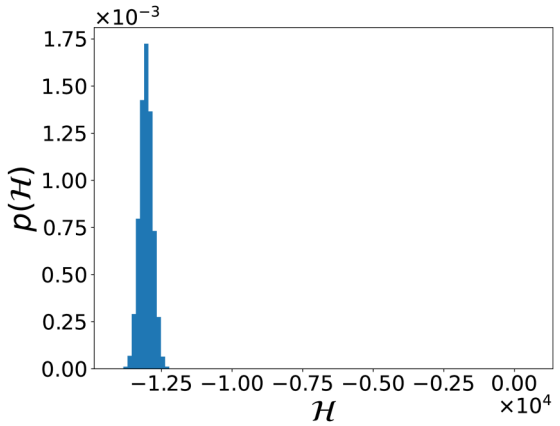

FIG. 7. Probability distribution for the outcome of the Ising model interaction Hamiltonian for a graph consisting of 1000 nodes with a connectivity of 10%.

Since our purpose here is to demonstrate the scalability of the unconditional method, we did not optimize the ramp strategy. However, as can be seen above, it is likely that an optimized ramp strategy would give a narrower distribution and a higher success rate, which is clearly desirable in finding the best solution.

VI. CONCLUSION

The coherent Ising machine is a promising, novel technology with potential applications in a number of areas. An advantage over classical computers for a specific problem has been claimed [3], although the role of quantum effects remains unclear. Unlike many candidates for gate array-type quantum computers, the CIM can be operated at room temperature and has very stable states. For the measurement-feedback architecture, the size of the CIM can be scaled up quite easily. While it is likely that quantum effects only play a minor role if at all in contemporary realizations of the CIM, entering a regime for which these become relevant could possibly lead to even better performance due to quantum tunneling and other effects.

In such a regime, precise and reliable simulation methods are required to better understand the role of quantum effects. We have derived two different methods, both utilizing the generally nonapproximate positive-P phase-space representation. The conditional, weighted method allows for the simulation of a single instance or run of a given measurement-feedback CIM. It fully "captures" the effect of the partial state collapse induced by the homodyne measurement process. The total master equation allows for the simulation of an average over a large number of independent runs of the CIM. Here, the state collapse operator is removed from the master equation through the averaging process. Though the two methods are quite different in the way they have been derived and in terms of their numerical implementation, we have demonstrated that they are in good agreement for the CIM considered here.

The latter method is several orders of magnitude faster compared to the conditional one. This comes at the price of being limited to predictions for an overage over multiple runs of the CIM. However, one would most likely be interested in the outcome of a CIM averaged over multiple runs anyway, making the total master equation method the more useful choice due to its significantly lower computational demand.

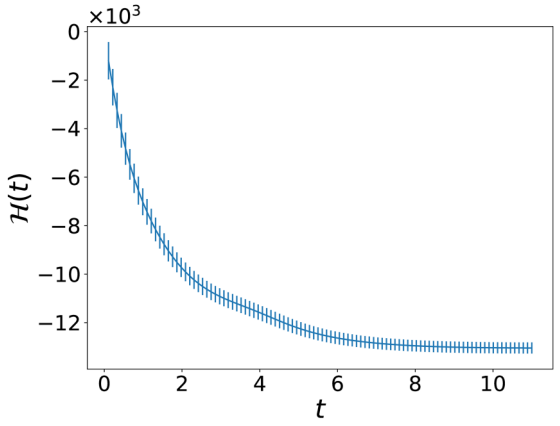

FIG. 8. Evolution of the mean Ising model interaction Hamiltonian for a graph consisting of 1000 nodes as a function of simulation time. Here, vertical lines indicate the standard deviation, obtained using $N_S = 102\,400$ stochastic trajectories.

ACKNOWLEDGMENTS

This work was partly performed on the OzSTAR national facility at Swinburne University of Technology. OzSTAR is funded by Swinburne University of Technology and the National Collaborative Research Infrastructure Strategy (NCRIS). This research was funded through a grant from NTT Phi Laboratories.

APPENDIX

Here we derive the form of the Stratonovich corrections for the feedback master equation. In general there are two terms, from measurement and from feedback.

Measurement

In the case of measurement, the operator $\mathcal{H}[c]\rho_c$ includes a mean value term, which means that it is nonlinear in the density matrix components. This leads to the additional terms described here. We only treat the single-mode case in this Appendix, as the multimode case is similar.

Writing out the B matrix for the single-mode case, and ignoring the k index since $k = 1$, we note that

$$B = \{\mathcal{H}[c]\rho_c\} = c\rho_c + \rho_c c^\dagger - T\rho_c, \tag{A1}$$

with the definition that $T \equiv \sum_{kl}[c_{lk} + c^\dagger_{lk}]\rho_{kl} \equiv \sum_{kl} t_{lk}\rho_{kl} = \langle c + c^\dagger\rangle_c$, provided that $\sum_k \rho_{kk} = 1$.

We now use an orthonormal basis expansion to transform the conditional density operator ρ_c into a matrix ρ_{mn}. The matrix derivative of the B matrix with respect to ρ_{mn} is given

by

$$\frac{\partial B_{ij}}{\partial \rho_{mn}} = \frac{\partial}{\partial \rho_{mn}}\left\{c_{ik}\rho_{kj} + \rho_{ik}c^{\dagger}_{kj} - \rho_{ij}\sum_{kl} t_{lk}\rho_{kl}\right\}$$
$$= \left\{c_{im}\delta_{jn} + \delta_{im}c^{\dagger}_{nj} - \delta_{im}\delta_{jn}T - \rho_{ij}t_{nm}\right\}. \quad \text{(A2)}$$

Therefore, we see immediately that the Stratonovich correction term $\mathrm{C}^{\mathcal{H}}$ is given by

$$C^{\mathcal{H}}_{ij} = -\frac{1}{2}\sum_{mn} B_{mn}\frac{\partial}{\partial \rho_{mn}}B_{ij}$$
$$= -\frac{1}{2}\sum_{mn}\left\{c_{mk}\rho_{kn} + \rho_{mk}c^{\dagger}_{kn} - \rho_{mn}T\right\}$$
$$\times\left\{c_{im}\delta_{jn} + \delta_{im}c^{\dagger}_{nj} - \delta_{im}\delta_{jn}T - \rho_{ij}t_{nm}\right\}. \quad \text{(A3)}$$

There are 12 terms in this product, and they are listed below:

(1) $c_{mk}\rho_{kn}c_{im}\delta_{jn} = c_{im}c_{mk}\rho_{kj} = (cc\rho_c)_{ij}$.
(2) $c_{mk}\rho_{kn}\delta_{im}c^{\dagger}_{nj} = c_{ik}\rho_{kn}c^{\dagger}_{nj} = (c\rho_c c^{\dagger})_{ij}$.
(3) $-c_{mk}\rho_{kn}\delta_{im}\delta_{jn}T = -c_{ik}\rho_{kj}T = -(c\rho_c T)_{ij}$.
(4) $-c_{mk}\rho_{kn}\rho_{ij}t_{nm} = -\rho_{ij}Tr(c\rho_c t)$.
(5) $\rho_{mk}c^{\dagger}_{kn}c_{im}\delta_{jn} = c_{im}\rho_{mk}c^{\dagger}_{kj} = (c\rho_c c^{\dagger})_{ij}$.
(6) $\rho_{mk}c^{\dagger}_{kn}\delta_{im}c^{\dagger}_{nj} = c^{\dagger}_{kn}\rho_{ik}c^{\dagger}_{nj} = (\rho_c c^{\dagger}c^{\dagger})_{ij}$.
(7) $-\rho_{mk}c^{\dagger}_{kn}\delta_{im}\delta_{jn}T = -c^{\dagger}_{kn}\rho_{ik}T = -(\rho_c c^{\dagger}T)_{ij}$.
(8) $-\rho_{mk}c^{\dagger}_{kn}\rho_{ij}t_{nm} = -\rho_{ij}Tr(t\rho_c c^{\dagger})$.
(9) $-\rho_{mn}Tc_{im}\delta_{jn} = -c_{im}T\rho_{mj} = -(Tc\rho_c)_{ij}$.
(10) $-\rho_{mn}T\delta_{im}c^{\dagger}_{nj} = -T\rho_{in}c^{\dagger}_{nj} = -(T\rho_c c^{\dagger})_{ij}$.
(11) $\rho_{mn}T\delta_{im}\delta_{jn}T = \rho_{ij}T^2$.
(12) $\rho_{mn}T\rho_{ij}t_{nm} = \rho_{ij}T(\rho_{mn}t_{nm}) = T\rho_{ij}Tr(\rho_c t)$.

Combining all these, and returning to an index-free operator notation, we obtain that

$$\mathrm{C}^{\mathcal{H}} = -\tfrac{1}{2}\big[cc\rho_c + 2c\rho_c c^{\dagger} + \rho_c c^{\dagger}c^{\dagger}$$
$$- 2T(c\rho_c + \rho_c c^{\dagger})$$
$$+ \rho_c T^2 + \rho_c Tr(T\rho_c t - c\rho_c t - t\rho_c c)\big]. \quad \text{(A4)}$$

The last term with factors of T is

$$T^2 + Tr(T\rho_c t - c\rho_c t - t\rho_c c^{\dagger}) = 2T^2 - \langle c^2 + c^{\dagger 2} + 2c^{\dagger}c\rangle. \quad \text{(A5)}$$

Combining terms together, one obtains that

$$\mathrm{C}^{\mathcal{H}} = \langle c + c^{\dagger}\rangle_c\mathcal{H}[c]\rho_c - c\rho_c c^{\dagger} + \rho_c\langle c^{\dagger}c\rangle - \tfrac{1}{2}\mathcal{H}[cc]\rho_c. \quad \text{(A6)}$$

Measurement and feedback

In the case of measurement with feedback, the operator multiplying the noise is $\xi(t)(\mathcal{H}+\mathcal{K})\rho_c$, where we will assume that $\mathcal{K}\rho_c \equiv [K, \rho_c]$. Writing out the B matrix for the single-mode case, we notice that

$$B = B^{\mathcal{H}} + B^{\mathcal{K}}$$
$$= c\rho_c + \rho_c c^{\dagger} - T\rho_c + K\rho_c - \rho_c K. \quad \text{(A7)}$$

The matrix derivative is

$$\frac{\partial B_{ij}}{\partial \rho_{mn}} = \frac{\partial}{\partial \rho_{mn}}\left\{B^{\mathcal{H}}_{ij} + [K\rho_c - \rho_c K]_{ij}\right\}$$
$$= \left\{B^{\mathcal{H}}_{ij,mn} + K_{im}\delta_{jn} - \delta_{im}K_{nj}\right\}. \quad \text{(A8)}$$

As a result, the total Stratonovich correction is

$$C_{ij} = C^{\mathcal{H}}_{ij} + C^{\mathcal{H}\mathcal{K}}_{ij} + C^{\mathcal{K}\mathcal{H}}_{ij} + C^{\mathcal{K}}_{ij},$$

where $C^{\mathcal{H}}$ was obtained already, and we obtain

$$C^{\mathcal{H}\mathcal{K}}_{ij} = -\frac{1}{2}\sum_{mn} B^{\mathcal{H}}_{mn}\frac{\partial}{\partial \rho_{mn}}B^{\mathcal{K}}_{ij}$$
$$= -\frac{1}{2}\sum_{mn}\left\{c_{mk}\rho_{kn} + \rho_{mk}c^{\dagger}_{kn} - \rho_{mn}T\right\}$$
$$\times\{K_{im}\delta_{jn} - \delta_{im}K_{nj}\}$$
$$= -\frac{1}{2}[K, c\rho_c + \rho_c c^{\dagger} - \rho_c T]_{ij}, \quad \text{(A9)}$$

$$C^{\mathcal{K}\mathcal{H}}_{ij} = -\frac{1}{2}\sum_{mn} B^{\mathcal{K}}_{mn}\frac{\partial}{\partial \rho_{mn}}B^{\mathcal{H}}_{ij}$$
$$= -\frac{1}{2}\sum_{mn}[K\rho_c - \rho_c K]_{mn}$$
$$\times\left\{c_{im}\delta_{jn} + \delta_{im}c^{\dagger}_{nj} - \delta_{im}\delta_{jn}T - \rho_{ij}t_{nm}\right\}$$
$$= -\frac{1}{2}\big[c[K, \rho_c] + [K, \rho_c]c^{\dagger}$$
$$- T[K, \rho_c] - \rho_c Tr[[K, \rho_c]t]\big]_{ij}, \quad \text{(A10)}$$

$$C^{\mathcal{K}}_{ij} = -\frac{1}{2}\sum_{mn} B^{\mathcal{K}}_{mn}\frac{\partial}{\partial \rho_{mn}}B^{\mathcal{K}}_{ij}$$
$$= -\frac{1}{2}\sum_{mn}[K, \rho_c]_{mn}\{K_{im}\delta_{jn} - \delta_{im}K_{nj}\}$$
$$= -\frac{1}{2}[K, [K, \rho_c]]_{ij}. \quad \text{(A11)}$$

Note that if $[c, K] = Q_1$ and $[c^{\dagger}, K] = Q_2$ with $Q_1, Q_2 \in \mathbb{C}$, it follows that

$$C^{\mathcal{K}\mathcal{H}}_{ij} = -\tfrac{1}{2}\big[Kc\rho_c - c\rho_c K + K\rho_c c^{\dagger} - \rho_c c^{\dagger}K + (Q_1 + Q_2)\rho_c$$
$$- T[K, \rho_c] - \rho_c Tr[\rho_c(Q_1 + Q_2)]\big]_{ij}$$
$$= C^{\mathcal{H}\mathcal{K}}_{ij}. \quad \text{(A12)}$$

We assume that these restrictions hold below.

Stratonovich master equation

Combining the terms given above, the Stratonovich-type master equation is

$$\dot{\rho}^{\mathrm{Strat}}_c = \mathcal{L}\rho_c + \mathcal{K}(c\rho_c + \rho_c c^{\dagger}) + \tfrac{1}{2}\mathcal{K}^2\rho_c$$
$$+ \mathrm{C}^{\mathcal{H}}\rho_c + 2C^{\mathcal{H}\mathcal{K}}\rho_c + C^{\mathcal{K}}\rho_c$$
$$+ \xi(t)\circ[\mathcal{H}[c] + \mathcal{K}]\rho_c, \quad \text{(A13)}$$

where the relevant corrections are

$$\mathrm{C}^{\mathcal{H}}\rho_c = \langle c + c^{\dagger}\rangle_c\mathcal{H}[c]\rho_c - c\rho_c c^{\dagger} + \rho_c\langle c^{\dagger}c\rangle - \tfrac{1}{2}\mathcal{H}[cc]\rho_c,$$
$$C^{\mathcal{H}\mathcal{K}}\rho_c = -\tfrac{1}{2}\big[K, c\rho_c + \rho_c c^{\dagger} - \rho_c T\big],$$
$$C^{\mathcal{K}}\rho_c = -\tfrac{1}{2}[K, [K, \rho_c]]. \quad \text{(A14)}$$

Since we are using the operators

$$c = \sqrt{2\gamma_m}a, \tag{A15}$$

$$K = \frac{\zeta}{\sqrt{2\gamma_m}}(a^\dagger - a), \tag{A16}$$

clearly $[c, K] = Q_1$ and $[c^\dagger, K] = Q_2$ with $Q_1, Q_2 \in \mathbb{C}$ are satisfied, from which it follows that $C^{\mathcal{HK}} = C^{\mathcal{KH}}$, hence

$$\begin{aligned}\dot{\rho}_c^{\text{Strat}} &= \mathcal{L}\rho_c + \mathcal{K}(c\rho_c + \rho_c c^\dagger) + \tfrac{1}{2}\mathcal{K}^2\rho_c \\ &\quad + \mathrm{C}^{\mathcal{H}}\rho_c + 2C^{\mathcal{HK}}\rho_c + C^{\mathcal{K}}\rho_c \\ &\quad + \xi(t)\circ[\mathcal{H}[c] + \mathcal{K}]\rho_c \\ &= \mathcal{L}\rho_c + T[K, \rho_c] + \mathrm{C}^{\mathcal{H}}\rho_c \\ &\quad + \xi(t)\circ[\mathcal{H}[c] + \mathcal{K}]\rho_c. \end{aligned} \tag{A17}$$

From this, we finally obtain that

$$\begin{aligned}\dot{\rho}_c^{\text{Strat}} &= \mathcal{L}\rho_c + c\rho_c c^\dagger - \rho_c\langle c^\dagger c\rangle - \tfrac{1}{2}\mathcal{H}[cc]\rho_c \\ &\quad + I_c(t)\circ[\mathcal{H}[c] + \mathcal{K}]\rho_c, \end{aligned} \tag{A18}$$

where

$$I_c(t) = \xi(t) + Tr[\rho_c(c + c^\dagger)]\,.$$

Multimode case

The above results can be generalized for a system comprised of N modes. In this case, there are N independent measurement noises $\xi_i(t)$. The B matrices are

$$\begin{aligned} B_r^{\mathcal{H}} &= c_r\rho + \rho c_r^\dagger - T_r\rho, \\ B_r^{\mathcal{K}} &= \sum_s J_{rs}(K_s\rho_c - \rho_c K_s), \end{aligned} \tag{A19}$$

with $T_r \equiv \sum_{kl}[c_{r;lk} + c_{r;lk}^\dagger]\rho_{r;kl} \equiv \sum_{kl} t_{r;lk}\rho_{r;kl} = \langle c_r + c_r^\dagger\rangle$. Note that in the multimode case, the operators are 3-tensors with the first index indicating the mode. The operators satisfy $c_{s;ik}\rho_{r;kj} = \rho_{r;ij}$ and $K_{s;ik}\rho_{r;kj} = \rho_{r;ij}$ which simplifies the calculations.

Analogously to the one-mode case, one finds

$$\begin{aligned} \mathrm{C}^{\mathcal{H}} &= \sum_r \langle c_r + c_r^\dagger\rangle\mathcal{H}[c_r]\rho_c + c_r\rho_c c_r^\dagger - \rho_c\langle c_r^\dagger c_r\rangle \\ &\quad - \frac{1}{2}\mathcal{H}[c_r c_r]\rho_c, \\ C^{\mathcal{HK}} &= -1\sum_{rs} J_{rs}\big[K_s, c_r\rho_c + \rho_c c_r^\dagger - \rho_c T_r\big], \\ C^{\mathcal{KH}} &= -\frac{1}{2}\sum_{rs}[c_r[K_s, \rho_c] + [K_s, \rho_c]c_r^\dagger \\ &\quad - T_r[K_s, \rho_c] - \rho_c Tr[[K_s, \rho_c]t_r]], \\ C^{\mathcal{K}} &= -\frac{1}{2}\sum_{rst} J_{rs}J_{rt}[K_r, [K_t, \rho_c]]. \end{aligned} \tag{A20}$$

[1] A. Lucas, Front. Phys. **2**, 5 (2014).
[2] F. W. Glover and G. A. Kochenberger, arXiv:1811.11538.
[3] T. Honjo, T. Sonobe, K. Inaba, T. Inagaki, T. Ikuta, Y. Yamada, T. Kazama, K. Enbutsu, T. Umeki, R. Kasahara *et al.*, Sci. Adv. **7**, eabh0952 (2021).
[4] P. L. McMahon, A. Marandi, Y. Haribara, R. Hamerly, C. Langrock, S. Tamate, T. Inagaki, H. Takesue, S. Utsunomiya, K. Aihara, R. L. Byer, M. M. Fejer, H. Mabuchi, and Y. Yamamoto, Science **354**, 614 (2016).
[5] P. D. Drummond and C. W. Gardiner, J. Phys. A: Math. Gen. **13**, 2353 (1980).
[6] P. Drummond, K. McNeil, and D. Walls, Opt. Acta **28**, 211 (1981).
[7] A. Gilchrist, C. W. Gardiner, and P. D. Drummond, Phys. Rev. A **55**, 3014 (1997).
[8] R. Schack and A. Schenzle, Phys. Rev. A **44**, 682 (1991).
[9] A. M. Smith and C. W. Gardiner, Phys. Rev. A **39**, 3511 (1989).
[10] M. R. Hush, A. R. R. Carvalho, and J. J. Hope, Phys. Rev. A **80**, 013606 (2009).
[11] S. Utsunomiya, K. Takata, and Y. Yamamoto, Opt. Express **19**, 18091 (2011).
[12] K. Takata, S. Utsunomiya, and Y. Yamamoto, New J. Phys. **14**, 013052 (2012).
[13] Z. Wang, A. Marandi, K. Wen, R. L. Byer, and Y. Yamamoto, Phys. Rev. A **88**, 063853 (2013).
[14] P. Drummond, K. McNeil, and D. Walls, Opt. Acta **27**, 321 (1980).
[15] E. Schrödinger, Naturwissenschaften **23**, 823 (1935).
[16] M. Wolinsky and H. J. Carmichael, Phys. Rev. Lett. **60**, 1836 (1988).
[17] L. Krippner, W. J. Munro, and M. D. Reid, Phys. Rev. A **50**, 4330 (1994).
[18] F. Böhm, G. Verschaffelt, and G. Van der Sande, Nat. Commun. **10**, 1 (2019).
[19] A. Marandi, Z. Wang, K. Takata, R. L. Byer, and Y. Yamamoto, Nat. Photonics **8**, 937 (2014).
[20] K. Takata, A. Marandi, R. Hamerly *et al.*, Sci. Rep. **6**, 34089 (2016).
[21] C. Wang, Y. Y. Gao, P. Reinhold, R. W. Heeres, N. Ofek, K. Chou, C. Axline, M. Reagor, J. Blumoff, K. M. Sliwa *et al.*, Science **352**, 1087 (2016).
[22] F.-X. Sun, Q. He, Q. Gong, R. Y. Teh, M. D. Reid, and P. D. Drummond, New J. Phys. **21**, 093035 (2019).
[23] F.-X. Sun, Q. He, Q. Gong, R. Y. Teh, M. D. Reid, and P. D. Drummond, Phys. Rev. A **100**, 033827 (2019).
[24] R. Y. Teh, F.-X. Sun, R. E. S. Polkinghorne, Q. Y. He, Q. Gong, P. D. Drummond, and M. D. Reid, Phys. Rev. A **101**, 043807 (2020).
[25] T. Shoji, K. Aihara, and Y. Yamamoto, Phys. Rev. A **96**, 053833 (2017).
[26] A. Yamamura, K. Aihara, and Y. Yamamoto, Phys. Rev. A **96**, 053834 (2017).
[27] T. Inagaki, Y. Haribara, K. Igarashi, T. Sonobe, S. Tamate, T. Honjo, A. Marandi, P. L. McMahon, T. Umeki, K. Enbutsu,

O. Tadanaga, H. Takenouchi, K. Aihara, K.-i. Kawarabayashi, K. Inoue, S. Utsunomiya, and H. Takesue, Science **354**, 603 (2016).
[28] S. J. Carter, P. D. Drummond, M. D. Reid, and R. M. Shelby, Phys. Rev. Lett. **58**, 1841 (1987).
[29] M. G. Raymer, P. D. Drummond, and S. J. Carter, Opt. Lett. **16**, 1189 (1991).
[30] P. D. Drummond and A. D. Hardman, Europhys. Lett. **21**, 279 (1993).
[31] P. D. Drummond, B. Opanchuk, A. Dellios, and M. D. Reid, Phys. Rev. A **105**, 012427 (2022).
[32] D. Maruo, S. Utsunomiya, and Y. Yamamoto, Phys. Scr. **91**, 083010 (2016).
[33] E. Wigner, Phys. Rev. **40**, 749 (1932).
[34] K. Takata, A. Marandi, and Y. Yamamoto, Phys. Rev. A **92**, 043821 (2015).
[35] Y. Inui and Y. Yamamoto, arXiv:2009.10328
[36] E. Ng, T. Onodera, S. Kako, P. L. McMahon, H. Mabuchi, and Y. Yamamoto, Phys. Rev. Research **4**, 013009 (2022).
[37] J. F. Corney and P. D. Drummond, Phys. Rev. A **68**, 063822 (2003).
[38] W. Lenz, Z. Phys. **21**, 613 (1920).
[39] E. Ising, Z. Phys. **31**, 253 (1925).
[40] Y. Yamamoto, K. Aihara, T. Leleu, K.-i. Kawarabayashi, S. Kako, M. Fejer, K. Inoue, and H. Takesue, npj Quantum Inf. **3**, 49 (2017).
[41] P. D. Drummond and M. Hillery, *The Quantum Theory of Nonlinear Optics* (Cambridge University Press, Cambridge, U.K., 2014).
[42] M. J. Werner, M. G. Raymer, M. Beck, and P. D. Drummond, Phys. Rev. A **52**, 4202 (1995).
[43] R. Hamerly, A. Marandi, M. Jankowski, M. M. Fejer, Y. Yamamoto, and H. Mabuchi, Phys. Rev. A **94**, 063809 (2016).
[44] A. Roy, R. Nehra, S. Jahani, L. Ledezma, C. Langrock, M. Fejer, and A. Marandi, Nat. Photonics **16**, 162 (2022).
[45] P. D. Drummond, J. D. Harvey, J. M. Dudley, D. B. Hirst, and S. J. Carter, Phys. Rev. Lett. **78**, 836 (1997).
[46] G. Patera, N. Treps, C. Fabre, and G. J. De Valcarcel, Eur. Phys. J. D **56**, 123 (2010).
[47] P. D. Drummond and S. Chaturvedi, Phys. Scr. **91**, 073007 (2016).
[48] C. W. Gardiner, *Handbook of Stochastic Methods for Physics, Chemistry, and the Natural Sciences* (Springer, Berlin, 2004).
[49] C. W. Gardiner, Phys. Rev. A **29**, 2814 (1984).
[50] H. J. Carmichael, *Statistical Methods in Quantum Optics 2: Non-classical Fields* (Springer, New York, 2009).
[51] Y. Yamamoto, T. Leleu, S. Ganguli, and H. Mabuchi, Appl. Phys. Lett. **117**, 160501 (2020).
[52] M. Stern, H. Sompolinsky, and L. F. Abbott, Phys. Rev. E **90**, 062710 (2014).
[53] H. M. Wiseman, Phys. Rev. A **49**, 2133 (1994).
[54] H. M. Wiseman and G. J. Milburn, Phys. Rev. Lett. **70**, 548 (1993).
[55] L. Diósi, Phys. Rev. A **40**, 1165 (1989).
[56] H. J. Carmichael, Phys. Rev. Lett. **70**, 2273 (1993).
[57] J. Dalibard, Y. Castin, and K. Mølmer, Phys. Rev. Lett. **68**, 580 (1992).
[58] K. Mølmer, Y. Castin, and J. Dalibard, J. Opt. Soc. Am. B **10**, 524 (1993).
[59] K. Kraus, Ann. Phys. **64**, 311 (1971).
[60] C. M. Caves and P. D. Drummond, Rev. Mod. Phys. **66**, 481 (1994).
[61] M. Hush, S. Szigeti, A. Carvalho, and J. Hope, New J. Phys. **15**, 113060 (2013).
[62] L. Diosi and N. Gisin, Phys. Rev. Lett. **72**, 4053 (1994).
[63] P. Bushev, D. Rotter, A. Wilson, F. Dubin, C. Becher, J. Eschner, R. Blatt, V. Steixner, P. Rabl, and P. Zoller, Phys. Rev. Lett. **96**, 043003 (2006).
[64] P. Deuar and P. D. Drummond, Phys. Rev. A **66**, 033812 (2002).
[65] P. Drummond and I. Mortimer, J. Comput. Phys. **93**, 144 (1991).
[66] H. Primas, in *Sixty-Two Years of Uncertainty: Historical, Philosophical, and Physical Inquiries into the Foundations of Quantum Mechanics*, edited by A. I. Miller (Springer, Boston, 1990), pp. 233–257.